Mechanostat-Informed Strain Mapping of Osseodensification-Inspired Peri-Implant Densification in Osteoporotic-Like Low-Density Cancellous Bone: A 3D Static Linear Finite Element Analysis

Mesut Tuzlali *, Nagehan Baki, Nazik İrem Önügören, Kübra Aral, Erkan Bahçe, Cüneyt Asım Aral

Posted Date: 18 February 2026

doi: 10.20944/preprints202602.1272.v1

Keywords: dental implants; osteoporosis; bone density; finite element analysis; biomechanical; mandible

 doi:10.20944/preprints202602.1272.v1

Article

Mechanostat-Informed Strain Mapping of Osseodensification-Inspired Peri-Implant Densification in Osteoporotic-Like Low-Density Cancellous Bone: A 3D Static Linear Finite Element Analysis

Mesut Tuzlali [1,*], Nagehan Baki [1], Nazik İrem Önügören [1], Kübra Aral [1], Erkan Bahçe [2] and Cüneyt Asım Aral [1]

[1] Inonu University, Faculty of Dentistry, Department of Prosthodontics, Malatya, Türkiye

[2] Inonu University, Faculty of Engineering, Department of Mechanical Engineering, Malatya, Türkiye

* Correspondence: mesut.tuzlali@inonu.edu.tr; Tel.: +90-422-222-05-00

Abstract

Background/Objectives: Low-density cancellous bone can amplify crestal cortical strain around implants because trabecular support is reduced. Osseodensification (OD) compacts trabecular bone and may create a peri-osteotomy densified zone, but its strain-level effects in osteoporotic-like bone are unclear. Given that osteoporosis/osteopenia in aging populations reduce trabecular support and can increase crestal cortical loading, this study tested whether an OD-inspired peri-implant densified trabecular zone lowers high-tail crestal cortical strains versus conventional drilling in an osteoporotic-like cancellous model. **Materials and Methods:** A 3D finite element mandibular posterior segment (2.0-mm cortical shell and D4 cancellous core) was modeled with a 4.3×11.4-mm titanium implant and a cemented monolithic zirconia crown. CD used a 4.0-mm osteotomy in D4 bone. OD used the same osteotomy plus an axially varying concentric densified shell (D1→D3 radially) with minor buccolingual cortical expansion. The implant–bone interface was bonded. Static 100 N loads were applied axially and obliquely (45°). Outcomes were εeq, εmax, and εmin, summarized as mean top-10 nodal values. **Results:** OD reduced crestal cortical strains under both loads. Axial loading: εeq 1470→1210 με (−17.7%), εmax 1420→1150 με (−19.0%), |εmin| 900→683 με (−24.1%). Oblique loading: εeq 3370→3040 με (−9.8%), εmax 2510→2310 με (−8.0%), |εmin| 3040→2770 με (−8.9%). Oblique loading produced higher cortical strains than axial loading in both models. **Conclusions:** OD-inspired peri-implant densification attenuated high-tail crestal cortical strain demand in this osteoporotic-like model, whereas off-axis loading remained the dominant driver of elevated strain. These findings support occlusal/prosthetic strategies that minimize oblique forces and warrant experimental and clinical validation.

Keywords: dental implants; osteoporosis; bone density; finite element analysis; biomechanical; mandible

1. Introduction

Bone-anchored devices are widely used across medicine, ranging from fracture fixation and spine instrumentation to craniofacial reconstruction and dental implant rehabilitation [1]. Despite differences in anatomy and loading environments, these systems share a common biomechanical determinant of success: stable load transfer at the bone–implant interface. In low-density cancellous (trabecular) bone, reduced structural support may increase local deformation and interfacial micromotion, which can compromise fixation and predispose to loosening or failure—phenomena well recognized in osteoporotic fixation contexts [2,3].

 doi:10.20944/preprints202602.1272.v1

Osteoporosis is a prevalent systemic skeletal disease and a leading contributor to fragility fractures in adults over 50 years of age [4]. With demographic aging, osteoporosis/osteopenia and related pharmacotherapy are increasingly encountered in patients seeking implant-based oral rehabilitation [5,6]. Systematic reviews and meta-analyses generally report no consistent reduction in dental implant survival attributable to osteoporosis alone, although modest differences in peri-implant marginal bone level changes have been observed across cohorts and the overall certainty of evidence remains limited [7,8]. In routine practice, risk assessment is also influenced by antiresorptive medications (e.g., bisphosphonates or denosumab) and their association with medication-related osteonecrosis of the jaw (MRONJ), highlighting the clinical value of understanding how low-density cancellous bone conditions can alter the local mechanical environment at the bone–implant interface [9–11].

In implant dentistry, low-density cancellous bone is a major risk factor for reduced primary stability and unfavorable early mechanical conditions [12]. Osseodensification (OD) was introduced as an alternative osteotomy preparation concept that compacts cancellous bone rather than removing it, with the intent of creating a localized densified peri-implant layer and improving mechanical purchase. Experimental work has reported increases in primary stability metrics and peri-implant bone mineral density and bone-to-implant contact when OD is compared with conventional subtractive drilling [13–15].

From a mechanobiological perspective, bone is a mechanosensitive tissue whose structure and mass adapt to the prevailing mechanical environment. The mechanostat framework proposed by Frost provides a widely used conceptual model linking tissue-level mechanical strain to bone modeling/remodeling responses, and it has been discussed in relation to osteopenia and osteoporosis [16–18]. In this context, strain-based descriptors can be clinically informative because they provide a direct measure of the local mechanical stimulus acting on cortical and cancellous compartments adjacent to an anchor device.

Although OD has been evaluated experimentally and clinically in terms of stability-related outcomes, the strain-level implications of an OD-associated densified peri-implant zone—especially under low-density (osteoporotic-like) cancellous conditions—remain insufficiently quantified using robust, distribution-aware post-processing [13,14,19]. A mechanostat-oriented strain mapping approach may help clarify whether peri-implant densification meaningfully shifts cortical entry-region strain concentrations and cancellous peri-implant strain patterns under functional loading directions [20].

Therefore, the aim of this study was to perform a mechanostat-informed, distribution-aware (high-tail) finite element evaluation of peri-implant densification inspired by osseodensification in an osteoporotic-like low-density cancellous bone model. Strain outcomes were summarized under axial and oblique loading.

2. Materials and Methods

Model Overview

A three-dimensional finite element model was developed to examine how an osseodensification-inspired peri-implant densified bone layer influences local strain distributions in a low-density (osteoporotic-like) cancellous mandibular segment under static loading. Two preparation conditions were evaluated: conventional drilling (CD) and osseodensification (OD). All modeling parameters were held constant between conditions except for the presence of the densified peri-implant zone and the minor cortical expansion described below.

Bone Segment Geometry

A posterior mandibular segment corresponding to the first molar region was created in SolidWorks 2024 (Dassault Systèmes, Vélizy-Villacoublay, France). The segment was idealized as a rectangular block measuring 20 mm (mesiodistal) × 8 mm (buccolingual) × 22 mm (vertical). A

 doi:10.20944/preprints202602.1272.v1

uniform 2.0-mm cortical shell surrounded a cancellous core. Gingival soft tissue was not included to reduce computational complexity and to focus the analysis on peri-implant bone mechanics. To avoid an artificially continuous cortical region at the segment ends, the mesial and distal cut faces were modeled without cortical coverage, while maintaining the cancellous core continuity.

Osteotomy Conditions

Two (primary) osteotomy preparation conditions were defined, with additional factor-isolation models to separate the mechanical contributions of peri-osteotomy trabecular densification and cortical expansion.

In the conventional drilling (CD) condition, a cylindrical osteotomy (4.0 mm diameter) was created and centered within the trabecular compartment. The cancellous bone was assigned low-density (D4) properties to represent a low-modulus trabecular substrate, while the cortical shell geometry and material properties were kept identical across all models.

In the osseodensification (OD) condition, the osteotomy diameter was maintained at 4.0 mm. To model OD-related compaction, a concentric circumferential densified trabecular shell was added along the osteotomy wall, consistent with histologic descriptions [13,14]. Specifically, osseodensification was modeled as a concentric, circumferential densified shell surrounding the implant osteotomy. The shell thickness was axially varying to mimic the reported gradient along the osteotomy, measuring 0.5 mm at the lateral (coronal) aspect and 1.0 mm at the apical aspect [13,14]. The native cancellous core in both models was assigned D4 properties to represent osteoporotic-like low-density cancellous bone; in the OD model, the peri-osteotomy shell was graded D1→D3 from inner to outer. To represent a stepwise increase in bone quality adjacent to the osteotomy, the densified shell was subdivided radially into three equal-thickness cancellous zones arranged from the osteotomy wall outward as D1 → D2 → D3. Thus, each zone thickness equaled 0.5/3 mm laterally and 1.0/3 mm apically, while preserving the same zonal order (D1 inner, D3 outer) throughout the shell. The term “osteoporotic-like” therefore refers to the low-modulus trabecular compartment (D4), while the cortical shell was kept constant across models to isolate the effect of peri-osteotomy trabecular densification. Additionally, a 0.2 mm buccolingual cortical expansion was incorporated in the OD model, increasing the external buccolingual dimension from 6.0 mm to 6.2 mm, in line with localized outward deformation reported during OD despite the limited intrinsic compressibility of cortical bone [13] (Figure 1).

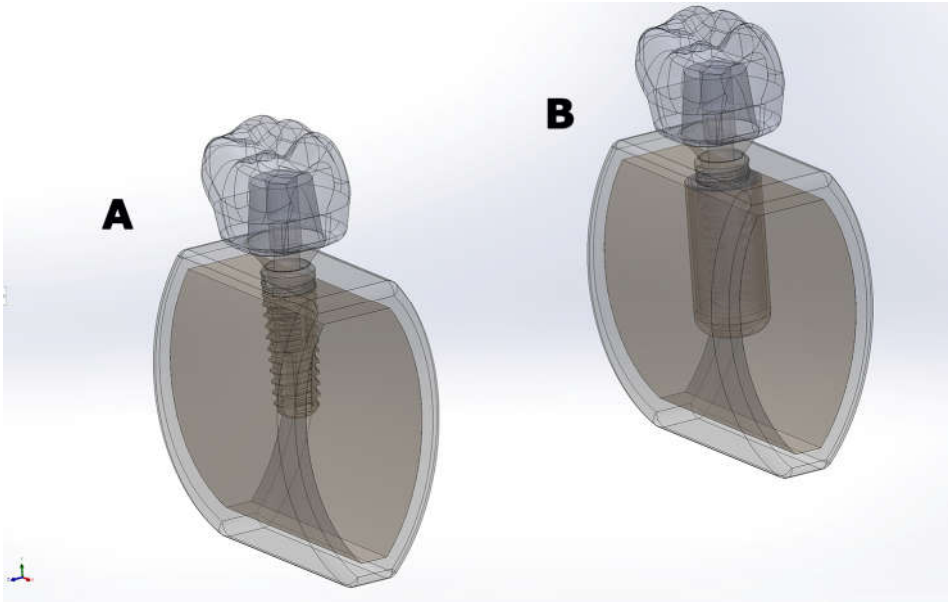

Figure 1. Finite element model geometries used in the analyses. (A) Conventional drilling (CD) model and (B) osseodensification (OD) model showing the implant–abutment–crown assembly embedded in the bone block

 doi:10.20944/preprints202602.1272.v1

(cortical and cancellous bone). The models differ in the osteotomy preparation protocol (CD vs OD), while all other geometric and material parameters were kept identical.

Implant–Restoration Assembly

A titanium dental implant (4.3 mm × 11.40 mm) with a thread cylindrical body and internal hex connection was modeled and positioned centrally within the bone segment, equidistant from the buccal and lingual cortical plates. A straight titanium abutment (6.5-mm diameter) with a 3.0-mm transmucosal height was connected to the implant via a modeled abutment screw reproducing the internal thread engagement geometry. A monolithic zirconia crown with mandibular first molar morphology was digitally designed and cemented to the abutment to approximate clinical loading transfer through a definitive restoration.

Material Properties

All materials were modeled as homogeneous, isotropic, and linearly elastic, as commonly adopted in implant finite element studies for comparative mechanical analyses. Material properties for titanium alloy (Ti-6Al-4V), zirconia, cortical bone, and cancellous bone were assigned according to the literature [21] and are summarized in Table 1. In the OD model, the densified trabecular layer was assigned a higher Young's modulus than the native trabecular core, consistent with micro-CT and histomorphometric evidence indicating increased peri-osteotomy mineral density/compaction after OD [13,22].

Table 1. Material properties.

Material	Modulus of elasticity (GPa)	Poisson's ratio (ν)
Cortical bone	14.8	0.30
Cancellous bone D1	9.5	0.30
Cancellous bone D2	5.5	0.30
Cancellous bone D3	1.6	0.30
Cancellous bone D4	0.69	0.30
Titanium (implant, abutment)	110	0.35
Zirconia	210	0.33

Meshing and Convergence

The assemblies were imported into ANSYS Workbench 2024 R2 (ANSYS Inc., Canonsburg, PA, USA). A tetrahedral mesh was generated with a 0.1-mm global element size and locally refined at the implant–crestal cortical region, where higher strain gradients were anticipated. In general, reducing element size (i.e., increasing mesh density) via progressive mesh refinement improves numerical accuracy and supports convergence toward an accurate solution, albeit at increased computational cost [23]. Mesh convergence was evaluated using three progressively refined global element sizes (0.5, 0.3, and 0.1 mm). Convergence was confirmed when the change in the peri-implant strain outcomes between successive refinements was ≤5%, and the 0.1-mm mesh was therefore adopted for all simulations. The final model comprised 5,837,993 nodes and 3,315,070 elements.

Contact Definitions and Boundary Conditions

Continuity between cortical and cancellous bone, and between densified and native cancellous bone in OD models, was enforced using shared nodes to preserve geometric and material continuity.

The implant–bone interface (cortical and trabecular) was defined as perfectly bonded, representing an idealized osseointegrated condition. For the two-piece implant configuration, the implant–abutment and abutment–screw interfaces were assigned bonded. The crown–abutment interface was also treated as bonded to represent a cemented connection. Screw preload was not modeled; interfaces were idealized as bonded to isolate the effect of peri-implant densification.

 doi:10.20944/preprints202602.1272.v1

To prevent rigid body motion and approximate fixation of the mandibular segment, the mesial and distal ends of the bone block were fully constrained in all degrees of freedom. The inferior surface was also fixed, providing global stabilization during load application. This constraint scheme was chosen to suppress rigid body motion and to provide consistent boundary conditions across models; outcomes were interpreted comparatively (OD vs CD) rather than as absolute physiologic magnitudes.

Loading Conditions

Two static loading configurations were simulated to represent posterior occlusal loading. For axial loading, a 100 N vertical force was applied perpendicular to the occlusal surface at the central fossa, distributed over an approximately 1 mm^2 contact area. For oblique loading, a 100 N force was applied at 45° to the implant's long axis and directed x, y, and z axes; it was applied over the same ~1 mm^2 central fossa contact area and resolved into orthogonal components along the global coordinate axes.

Outcome Measures and Strain Post-Processing

Primary outcomes were strain-based metrics in the peri-implant cortical region, including Equivalent (von Mises) elastic strain (ε_{eq}), maximum principal elastic strain (ε_{max}; tensile), and minimum principal elastic strain (ε_{min}; compressive).

To reduce the influence of localized numerical spikes arising from geometric transitions, contact edges, or mesh-related singularities, results were not interpreted using single-point maxima. Instead, strain data were exported from ANSYS Workbench and processed externally. For each region of interest, a high-tail descriptor was calculated as the mean value of the 10 nodes exhibiting the highest strain magnitudes, thereby mitigating the effect of numerical artifacts while preserving sensitivity to peak mechanical demand. Post-processing was performed using Microsoft Excel (Microsoft Corp., Redmond, WA, USA).

All strain values were reported as dimensionless strain (mm/mm) and additionally expressed in microstrain (με) for interpretability (με = strain × 10^6). Comparative evaluation between CD and OD models was performed by examining the magnitude and spatial distribution of strain fields under axial and oblique loading, supported by contour maps and percentile summaries.

3. Results

The results are presented as comparative cortical strain outcomes for the CD and OD models under axial and oblique loading. Detailed findings are reported by strain metric in the following subsections.

3.1. Cortical Bone Strain Outcomes

Peri-implant cortical bone strain was consistently lower in the OD model than in the CD model under both loading directions (Table 2; Figures 2–5). Strain concentrations were located primarily in the crestal cortical bone surrounding the implant. Values are reported in microstrain (με), where 1 με = 10^{-6} strain (mm/mm).

Table 2. Mean high-tail peri-implant cortical bone elastic strain under axial and oblique loading (top-10 node averaging). Values are reported in microstrain (με). Negative values indicate compressive strain. For ε_{eq} and ε_{max}, the mean of the 10 nodes exhibiting the highest strain values within the cortical region of interest (ROI) was computed. For ε_{min}, the mean of the 10 nodes exhibiting the most negative (i.e., most compressive) strain values was computed. Percentage change (Δ%) was calculated as (OD − CD)/CD × 100 for ε_{eq} and ε_{max}. For ε_{min}, Δ% was calculated using strain magnitudes: (|OD| − |CD|)/|CD| × 100.

Strain measure (cortical bone)	Axial loading			Oblique loading		
	CD (με)	OD (με)	Δ%	CD (με)	OD (με)	Δ%

 doi:10.20944/preprints202602.1272.v1

Equivalent von Mises elastic strain, ε_{eq}	1470	1210	-17.7%	3370	3040	-9.8%
Maximum principal elastic strain, ε_{max}	1420	1150	-19.0%	2510	2310	-8.0%
Minimum principal elastic strain, ε_{min}	-900	-683	-24.1%	-3040	-2770	-8.9%

CD, conventional drilling; OD, osseodensification. For ε_{eq} and ε_{max}, high-tail strain was defined as the mean of the 10 highest nodal values; for ε_{min}, as the mean of the 10 most compressive nodal values. Percentage change (Δ%) was calculated as described in the Methods.

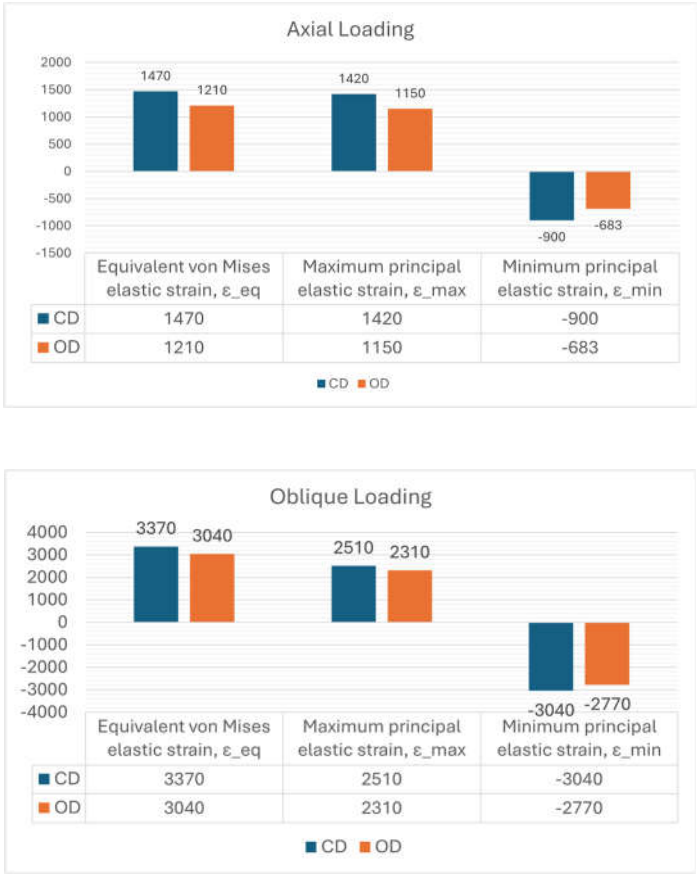

Figure 2. Mean peak peri-implant cortical bone elastic strain under (A) axial and (B) oblique loading for CD and OD models. Values are reported in microstrain (με); negative values indicate compressive strain. For each outcome, the mean of the 10 nodes representing the high-tail response (as defined in Table 2) was computed.

 doi:10.20944/preprints202602.1272.v1

Models	Cortical Bone Equivalent von Mises Elastic Strain	
	Axial Loading	Oblique Loading
CD / OD	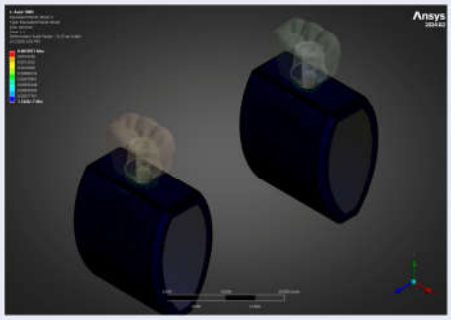	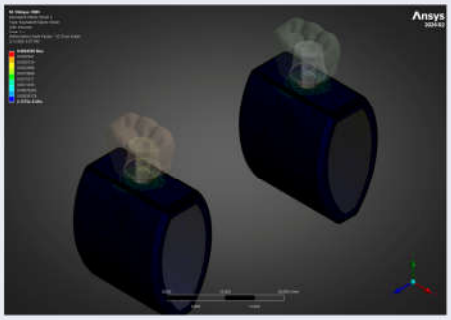

Figure 3. Cortical bone equivalent (von Mises) elastic strain (ε_{eq}) contours for CD and OD models under (A) axial and (B) oblique loading. Contours are displayed in mm/mm (1 mm/mm = 10^6 με).

Models	Cortical Bone Maximum Principal Elastic Strain	
	Axial Loading	Oblique Loading
CD / OD	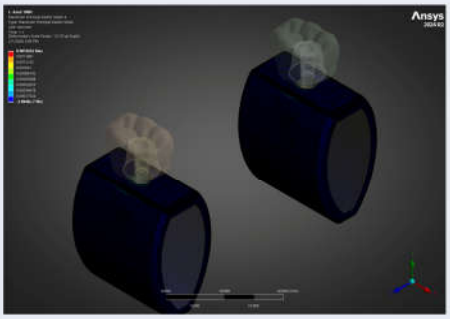	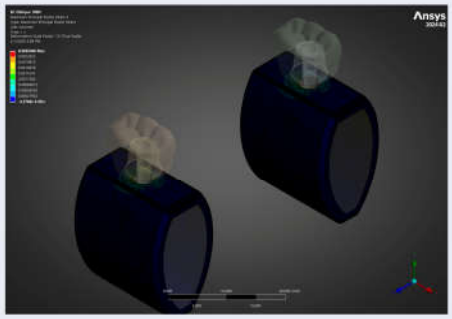

Figure 4. Cortical bone maximum principal elastic strain (ε_{max}) contours for CD and OD models under (A) axial loading and (B) oblique loading. Contours are displayed in mm/mm (1 mm/mm = 10^6 με).

Models	Cortical Bone Minimum Principal Elastic Strain	
	Axial Loading	Oblique Loading
CD / OD	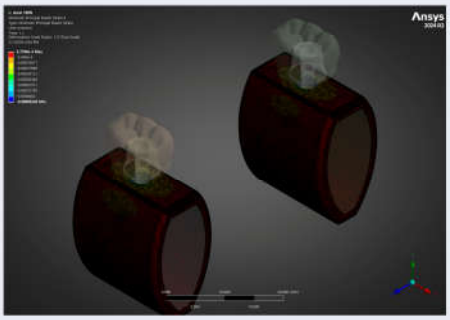	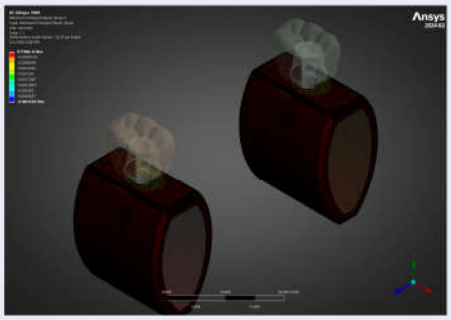

 doi:10.20944/preprints202602.1272.v1

Figure 5. Cortical bone minimum principal elastic strain (ε_{min}) contours for CD and OD models under (A) axial loading and (B) oblique loading. Contours are displayed in mm/mm (1 mm/mm = 10^6 με); negative values indicate compressive strain.

3.2. Equivalent (von Mises) Elastic Strain

Under axial loading (100 N), the mean high-tail εeq decreased from 1470 με in CD to 1210 με in OD (Δ = −260 με; −17.7%). Under oblique loading (100 N at 45°), εeq decreased from 3370 με (CD) to 3040 με (OD) (Δ = −330 με; −9.8%) (Figure 3).

3.3. Maximum Principal (Tensile) Elastic Strain

For axial loading, εmax decreased from 1420 με (CD) to 1150 με (OD) (Δ = −270 με; −19.0%). For oblique loading, εmax decreased from 2510 με (CD) to 2310 με (OD) (Δ = −200 με; −8.0%) (Figure 4).

3.4. Minimum Principal (Compressive) Elastic Strain

Compressive strain magnitudes were lower in the OD model. Under axial loading, εmin changed from −900 με (CD) to −683 με (OD), corresponding to a 24.1% reduction in compressive strain magnitude (|εmin|). Under oblique loading, εmin changed from −3040 με (CD) to −2770 με (OD), corresponding to an 8.9% reduction in |εmin| (Figure 5).

4. Discussion

This finite element analysis investigated whether an osseodensification (OD)–inspired peri-osteotomy densified trabecular zone can meaningfully shift peri-implant strain demand in a low-stiffness ("osteoporotic-like") cancellous environment. Under both axial and 45° oblique loading, the OD model consistently reduced high-tail strain metrics in the crestal cortical region compared with conventional drilling (CD), with a larger relative effect under axial loading (~18–24% depending on metric) and a smaller but directionally consistent effect under oblique loading (~8–10%). These findings support the biomechanical plausibility that locally increasing peri-implant trabecular stiffness—conceptually consistent with OD-associated densification—can partially offload the crestal cortical collar, a region widely recognized as a mechanical hotspot under bending-dominant loading [16,24].

Mechanostat-Informed Interpretation of Peri-Implant Strain Magnitudes

Interpreting peri-implant strain in the context of bone mechanoregulation is useful when it is framed as a relative stimulus indicator rather than a direct surrogate for clinical failure. Frost's mechanostat framework proposes broad strain "windows" in which bone tends to maintain, model, or remodel, with increases in modeling becoming more likely as strains enter the ~1500–3000 με range in vivo (noting that such thresholds are conceptual and context-dependent). For reference, commonly cited mechanostat thresholds were considered: disuse (≤~50–100 με), adapted window (~1000–1500 με), overload (~1500–3000 με), and pathological overload (≥~3000 με); fracture/failure has been reported only at substantially higher strain levels (often ≥~15000 με) [16,25].

In the present model, oblique loading drove the crestal cortical region into a higher strain regime than axial loading, consistent with the expectation that lateral components generate bending moments and concentrate deformation cervically. Within this framework, the OD-inspired densification shifted high-tail crestal cortical strains downward under both load directions, suggesting a mechanical environment with a reduced probability of operating in a high-strain "upper-tail" state—particularly relevant when bone quality is low and trabecular load sharing is diminished.

Experimental mechanobiology further indicates that skeletal adaptation is sensitive not only to strain magnitude but also to features of the stimulus such as cycle structure and rest insertion, and

 doi:10.20944/preprints202602.1272.v1

that adaptive responses can behave in an approximately monotonic/near-linear manner across broad ranges between disuse- and high-strain conditions [17].

Accordingly, the present results should be interpreted as evidence of a directionally favorable redistribution of strain demand at the crestal cortical region rather than as a predictor of marginal bone loss or a "safe/unsafe" threshold exceedance.

Relationship to the Osseodensification Evidence Base

OD has primarily been positioned as a site-preparation approach intended to preserve and compact bone, creating a densified layer at the osteotomy wall and improving mechanical engagement—effects that have been supported by preclinical and clinical observations. Histologic and/or micro-CT–supported reports have described peri-osteotomy densification patterns and improved stability-related outcomes consistent with the conceptual mechanism of OD [13,14,26].

In vivo, a multicenter controlled clinical trial reported higher insertion torque and favorable temporal stability quotient (ISQ) behavior with OD relative to subtractive drilling across varying implant designs and site characteristics [15]

Systematic syntheses likewise conclude that OD tends to improve primary stability surrogates and may increase local densification markers, while emphasizing heterogeneity in protocols, outcomes, and the relative scarcity of long-term, hard-endpoint clinical evidence [19,27,28].

Within this context, the present study contributes a complementary, strain-based perspective: rather than focusing on insertion torque or ISQ as primary endpoints, it quantifies how a densified peri-osteotomy zone may alter functional strain demand in the crestal cortical collar. Mechanically, increasing peri-implant trabecular stiffness promotes improved load sharing around the osteotomy wall and may reduce the concentration of deformation at the cortical crest, particularly when the loading direction is predominantly axial. The smaller effect under oblique loading is also mechanically intuitive: bending moments amplify crestal deformation even when trabecular support is stiffened, implying that densification may not fully mitigate off-axis overload.

Why the Crestal Cortical Region Is a Critical Area in Low-Density Cancellous Bone

When cancellous stiffness is reduced, the cortical shell can bear a disproportionate share of load, increasing local strain gradients at the crestal collar under functional loading. This theme is consistent with broader orthopedic discussions of fixation mechanics in osteoporotic bone, where reduced bone quality can amplify interface deformation demands [2,3].

In implant dentistry, this concept also intersects with immediate/early loading biomechanics, where excessive implant–bone micromotion has been implicated in fibrous encapsulation risk and where stable mechanical conditions are emphasized as a prerequisite for predictable osseointegration [29,30].

Although the present simulations assumed a perfectly bonded (osseointegrated) interface, the observed reduction in high-tail cortical region strains in the OD model supports the hypothesis that a densified peri-osteotomy zone could provide a mechanical "buffer" in compromised cancellous environments—while still leaving oblique loading as the dominant driver of peak crestal strain demand.

Clinical Implications and Cautious Translation

Clinically, OD is often selected in low-quality bone to enhance primary stability. The present findings provide a plausible mechanical complement: if peri-osteotomy densification increases effective local stiffness, crestal cortical strain concentrations under functional loads may be reduced, potentially moderating mechanically driven remodeling stimuli at the cortical collar [15,16].

However, translation should remain cautious. A static, linear-elastic, fully bonded model does not account for time-dependent remodeling, viscoelasticity, partial integration, or cyclic fatigue. Moreover, posterior bite forces can substantially exceed 100 N depending on patient factors and

 doi:10.20944/preprints202602.1272.v1

measurement conditions; therefore, the present loads should be interpreted as standardized comparative probes rather than as patient-specific physiologic maxima [31].

From a clinical biomechanics' standpoint, the strong load-direction dependence observed here reinforces that occlusal and prosthetic strategies that reduce off-axis forces (e.g., occlusal scheme optimization, cusp guidance control, cantilever management, and stiffness/splinting considerations) remain fundamental adjuncts to any osteotomy-based approach.

Limitations and Future Research Directions

Several limitations typical of implant FEA should be acknowledged. First, bone was modeled as homogeneous, isotropic, and linearly elastic, and the mandibular segment geometry and boundary constraints were simplified. Second, complete osseointegration was assumed via a perfectly bonded implant–bone interface; this is appropriate for evaluating post-integration load transfer but does not represent early healing conditions where frictional contact, partial integration, and micromotion are central. Third, loading was static and applied at a single occlusal contact region; in vivo loading is cyclic and multi-contact, and stimulus history (including rest insertion and frequency structure) influences adaptation [17]. Fourth, the OD condition was idealized by prescribing a graded peri-osteotomy material zone and a minor cortical expansion; this captures the intended mechanical consequence (increased peri-implant stiffness) but does not simulate the drilling process, potential microdamage, thermal effects, or patient-specific heterogeneity in densification patterns.

Future studies should therefore (i) incorporate CT-based heterogeneous material mapping and, where feasible, anisotropy; (ii) evaluate a range of densified-zone thicknesses/gradients and modulus ratios to quantify robustness; (iii) add cyclic loading and/or mechanobiologic remodeling formulations; and (iv) compare bonded versus frictional/contact interfaces to estimate micromotion and early-stage stability metrics. Finally, validation against experimental strain measurements or calibrated low-density cancellous bone analog models would strengthen translational interpretability. Broadly, adopting reporting structure consistent with contemporary in-silico guidelines (RIFEM) and implant-FEA best-practice recommendations would further improve reproducibility [24,32].

5. Conclusions

Within the limitations of this idealized, fully osseointegrated finite element model representing osteoporotic-like low-density cancellous bone, an OD-inspired graded peri-implant densified trabecular zone consistently reduced the high-tail crestal cortical region strain response under both axial and 45° oblique loading, with a larger relative reduction under axial loading (~18–24%) than under oblique loading (~8–10%). Oblique loading remained the dominant driver of elevated crestal cortical strains, underscoring that off-axis load management is central in low-density cancellous bone even when peri-implant densification is achieved. Overall, these findings provide biomechanical support for the plausibility of peri-implant densification as a strategy to attenuate crestal cortical deformation, while highlighting the need for experimental validation and standardized, distribution-aware post-processing to improve reproducibility and clinical translation.

Author Contributions: Conceptualization, M.T., N.B., and K.A.; methodology, M.T., C.A.A., and E.B.; software, M.T. and E.B.; validation, M.T., N.İ.Ö., and E.B.; formal analysis, M.T. and E.B.; investigation, M.T., K.A., C.A.A.; resources, M.T., N.B., and C.A.A; data curation, M.T. and E.B.; writing—original draft preparation M.T. and N.B.; writing—review and editing, M.T., N.B., K.A, N.İ.Ö., and E.B.; visualization, M.T.; supervision, C.A.A..; project administration, M.T.

Funding: This research received no external funding.

Institutional Review Board Statement: Not applicable.

Informed Consent Statement: Not applicable.

 doi:10.20944/preprints202602.1272.v1

Data Availability Statement: The datasets used and/or analyzed during the current study are available from the corresponding author on reasonable request.

Acknowledgments: During the preparation of this manuscript/study, the authors used Google Translate, DeepL, ChatGPT, PaperPal, and Grammarly for the purposes of enhancing language clarity and accuracy. The authors have reviewed and edited the output and take full responsibility for the content of this publication.

Conflicts of Interest: The authors declare no conflicts of interest.

Abbreviations

The following abbreviations are used in this manuscript:

BMD	Bone mineral density
CD	Conventional drilling
D1–D4	Cancellous bone density classes (Lekholm & Zarb classification)
FEA	Finite element analysis
ISQ	Implant stability quotient
MRONJ	Medication-related osteonecrosis of the jaw
OD	Osseodensification
ROI	Region of interest
ε_{eq}	Equivalent (von Mises) elastic strain
ε_{max}	Maximum principal (tensile) elastic strain
ε_{min}	Minimum principal (compressive) elastic strain
με	Microstrain (10^{-6} strain)

References

1. Isaacson BM, Jeyapalina S. Osseointegration: a review of the fundamentals for assuring cementless skeletal fixation. Orthopedic Research and reviews. 2014;2014(6):55-65.
2. Mukhopadhaya J, Bhadani JS. Fixation Failure in Osteoporotic Bone: A Review of Complications and Outcomes. Indian J Orthop. 2025;59(3):389-404.
3. Tandon V, Franke J, Kalidindi KKV. Advancements in osteoporotic spine fixation. J Clin Orthop Trauma. 2020;11(5):778-85.
4. Sözen T, Özışık L, Başaran N. An overview and management of osteoporosis. Eur J Rheumatol. 2017;4(1):46-56.
5. Shen Y, Huang X, Wu J, Lin X, Zhou X, Zhu Z, et al. The Global Burden of Osteoporosis, Low Bone Mass, and Its Related Fracture in 204 Countries and Territories, 1990-2019. Front Endocrinol (Lausanne). 2022;13:882241.
6. Sànchez-Riera L, Wilson N, Kamalaraj N, Nolla JM, Kok C, Li Y, et al. Osteoporosis and fragility fractures. Best Pract Res Clin Rheumatol. 2010;24(6):793-810.
7. de Medeiros F, Kudo GAH, Leme BG, Saraiva PP, Verri FR, Honório HM, et al. Dental implants in patients with osteoporosis: a systematic review with meta-analysis. Int J Oral Maxillofac Surg. 2018;47(4):480-91.
8. Lemos CAA, de Oliveira AS, Faé DS, Oliveira H, Del Rei Daltro Rosa CD, Bento VAA, et al. Do dental implants placed in patients with osteoporosis have higher risks of failure and marginal bone loss compared to those in healthy patients? A systematic review with meta-analysis. Clin Oral Investig. 2023;27(6):2483-93.
9. Seo DD, Borke JL. Medication-Related Osteonecrosis of the Jaw–2024 Update. Oral Health Dental Sci. 2024;8(1):1-6.
10. Andersen SWM, Hindocha NV, Poulsen I, Schliephake H, Jensen SS. Medication-Related Osteonecrosis of the Jaws in Patients on Antiresorptive Medication With Dental Implants. A Scoping Review. Clin Oral Implants Res. 2025;36(10):1173-201.

 doi:10.20944/preprints202602.1272.v1

11. Ruggiero SL, Dodson TB, Aghaloo T, Carlson ER, Ward BB, Kademani D. American Association of Oral and Maxillofacial Surgeons' Position Paper on Medication-Related Osteonecrosis of the Jaws-2022 Update. J Oral Maxillofac Surg. 2022;80(5):920-43.
12. O'Sullivan D, Sennerby L, Jagger D, Meredith N. A comparison of two methods of enhancing implant primary stability. Clin Implant Dent Relat Res. 2004;6(1):48-57.
13. Huwais S, Meyer EG. A Novel Osseous Densification Approach in Implant Osteotomy Preparation to Increase Biomechanical Primary Stability, Bone Mineral Density, and Bone-to-Implant Contact. Int J Oral Maxillofac Implants. 2017;32(1):27-36.
14. Trisi P, Berardini M, Falco A, Podaliri Vulpiani M. New Osseodensification Implant Site Preparation Method to Increase Bone Density in Low-Density Bone: In Vivo Evaluation in Sheep. Implant Dent. 2016;25(1):24-31.
15. Bergamo ETP, Zahoui A, Barrera RB, Huwais S, Coelho PG, Karateew ED, Bonfante EA. Osseodensification effect on implants primary and secondary stability: Multicenter controlled clinical trial. Clin Implant Dent Relat Res. 2021;23(3):317-28.
16. Frost HM. Bone's mechanostat: a 2003 update. Anat Rec A Discov Mol Cell Evol Biol. 2003;275(2):1081-101.
17. Sugiyama T, Meakin LB, Browne WJ, Galea GL, Price JS, Lanyon LE. Bones' adaptive response to mechanical loading is essentially linear between the low strains associated with disuse and the high strains associated with the lamellar/woven bone transition. J Bone Miner Res. 2012;27(8):1784-93.
18. Marques FC, Boaretti D, Walle M, Scheuren AC, Schulte FA, Müller R. Mechanostat parameters estimated from time-lapsed in vivo micro-computed tomography data of mechanically driven bone adaptation are logarithmically dependent on loading frequency. Front Bioeng Biotechnol. 2023;11:1140673.
19. Fontes Pereira J, Costa R, Nunes Vasques M, Salazar F, Mendes JM, Infante da Câmara M. Osseodensification: An Alternative to Conventional Osteotomy in Implant Site Preparation: A Systematic Review. J Clin Med. 2023;12(22).
20. Meslier QA, Shefelbine SJ. Using Finite Element Modeling in Bone Mechanoadaptation. Curr Osteoporos Rep. 2023;21(2):105-16.
21. Premnath K, Sridevi J, Kalavathy N, Nagaranjani P, Sharmila MR. Evaluation of stress distribution in bone of different densities using different implant designs: a three-dimensional finite element analysis. J Indian Prosthodont Soc. 2013;13(4):555-9.
22. Lahens B, Neiva R, Tovar N, Alifarag AM, Jimbo R, Bonfante EA, et al. Biomechanical and histologic basis of osseodensification drilling for endosteal implant placement in low density bone. An experimental study in sheep. J Mech Behav Biomed Mater. 2016;63:56-65.
23. Pisarciuc C, Dan I, Cioară R. The Influence of Mesh Density on the Results Obtained by Finite Element Analysis of Complex Bodies. Materials (Basel). 2023;16(7).
24. Falcinelli C, Valente F, Vasta M, Traini T. Finite element analysis in implant dentistry: State of the art and future directions. Dent Mater. 2023;39(6):539-56.
25. Frost HM. Bone "mass" and the "mechanostat": a proposal. Anat Rec. 1987;219(1):1-9.
26. Lahens B, Lopez CD, Neiva RF, Bowers MM, Jimbo R, Bonfante EA, et al. The effect of osseodensification drilling for endosteal implants with different surface treatments: A study in sheep. J Biomed Mater Res B Appl Biomater. 2019;107(3):615-23.
27. Turner CH. Three rules for bone adaptation to mechanical stimuli. Bone. 1998;23(5):399-407.
28. Warden SJ, Hurst JA, Sanders MS, Turner CH, Burr DB, Li J. Bone adaptation to a mechanical loading program significantly increases skeletal fatigue resistance. J Bone Miner Res. 2005;20(5):809-16.
29. Szmukler-Moncler S, Salama H, Reingewirtz Y, Dubruille JH. Timing of loading and effect of micromotion on bone-dental implant interface: review of experimental literature. J Biomed Mater Res. 1998;43(2):192-203.
30. Szmukler-Moncler S, Piattelli A, Favero GA, Dubruille JH. Considerations preliminary to the application of early and immediate loading protocols in dental implantology. Clin Oral Implants Res. 2000;11(1):12-25.
31. Koc D, Dogan A, Bek B. Bite force and influential factors on bite force measurements: a literature review. Eur J Dent. 2010;4(2):223-32.

 doi:10.20944/preprints202602.1272.v1

32. Mathur VP, Atif M, Duggal I, Tewari N, Duggal R, Chawla A. Reporting guidelines for in-silico studies using finite element analysis in medicine (RIFEM). Comput Methods Programs Biomed. 2022;216:106675.